

Electrochemical studies of zinc–cobalt alloy coatings deposited from alkaline baths containing glycine as complexing agent

M. Heydari Gharahcheshmeh · M. Heydarzadeh Sohi

Received: 5 May 2009 / Accepted: 18 April 2010 / Published online: 13 May 2010
© Springer Science+Business Media B.V. 2010

Abstract Co-deposition of Zn–Co alloy coatings that were electrodeposited from weakly alkaline glycine solutions has been studied by cyclic voltammetry. Scanning electron microscopy (SEM), energy dispersive spectroscopy (EDS), and X-ray diffraction (XRD) analyses were used to study surface morphology, chemical composition, and phase structure of the coatings. Corrosion behavior of the coatings was also studied using potentiodynamic polarization tests in 3.5 wt% NaCl solution. Cyclic voltammetry results showed that in Zn–Co deposition from an alkaline bath in the presence of glycine, cobalt deposited at a potential near to that of zinc together with successful co-deposition of Co and Zn. It was also shown that reduction–oxidation (redox) reactions of Zn–Co alloy deposits were quasi-reversible and resulted in deviation of electrodeposited alloys from the equilibrium phase diagrams. The corrosion resistance of the deposits was also highly influenced by the composition and morphology of the coatings. Overall, Zn–Co deposit containing 0.89 wt% Co showed that the highest corrosion resistance among the coatings that was due to its single phase structure and fine morphology.

Keywords Zn–Co · Electrodeposition · Cyclic voltammetry · Corrosion

M. H. Gharahcheshmeh · M. H. Sohi (✉)
School of Metallurgy and Materials Engineering, College
of Engineering, University of Tehran, Tehran, Iran
e-mail: mhsahi@ut.ac.ir

M. H. Gharahcheshmeh
e-mail: mheydari@ut.ac.ir

1 Introduction

The interest in zinc alloy electrodeposits has been growing as a consequence of their higher corrosion resistance and better mechanical characteristics in comparison with pure zinc coatings [1–5]. They can also be considered as substitutes for toxic and high-cost cadmium coatings [5–8].

The co-deposition process of zinc together with metals of the iron group (Ni, Co, and Fe), has been observed to be anomalous in many cases, because the less noble metal, i.e., zinc, is deposited preferentially on the cathode with respect to the more noble metals [9–17]. Several theories have been suggested by various researchers about anomalous co-deposition. The most widespread theory in this regard is the so-called hydroxide suppression mechanism (HSM) [10, 14, 17].

The electrodeposition of zinc and zinc alloys is usually conducted in both acidic and alkaline solutions [18–21]. Most of the commercial alkaline baths used for electroplating of zinc and zinc alloys contain cyanide compounds which are both toxic and corrosive [19, 20].

The use of organic additives in electrodeposition bath is extremely important due to their influence on the growth and structure of the deposits obtained [22–25]. Barbosa and Carlos [26] used sorbitol as a complex agent in alkaline bath applied for deposition of Zn–Fe. They observed that sorbitol had a beneficial effect in minimizing the potential difference of iron and zinc, and hence successful co-deposition of Fe and Zn. Mouanga et al. [24] used coumarin in an acidic bath applied for the deposition of Zn–Co. They found that coumarin affected the reduction of zinc, but it had no effect on the reduction of cobalt. They also noticed that the presence of coumarin in the electrolyte resulted in structural refinement of alloy deposits and increase of cathodic current efficiency. Ballesteros et al.

[27] studied the influence of polyethylene glycol 20000 (PEG₂₀₀₀₀) on the mechanism of zinc deposition. They observed that zinc reduction potential moved to more negative values in the presence of PEG₂₀₀₀₀ without significant interference from the hydrogen evolution reaction.

In this research, electrodeposition of Zn–Co alloys from a cyanide free alkaline bath in the presence of glycine as a complexing agent was studied using direct current. Cyclic voltammetry was also used to study co-deposition of zinc and cobalt. Scanning electron microscopy (SEM), energy dispersive spectroscopy (EDS), and X-ray diffraction (XRD) analyses of Zn–Co films were applied to determine the morphology, composition, and structure of the coatings, respectively. Finally, the corrosion behaviors of Zn–Co alloy coatings were also studied to find the optimum cobalt content in the coating.

2 Experimental

AISI 1018 steel specimens with a plated area of 2 cm × 1 cm and high purity zinc were used as cathode and anode, respectively. Before electroplating commencement, the samples were polished and thoroughly degreased in alkaline solution (containing 10 g L⁻¹ NaOH and 40 g L⁻¹ Na₂CO₃) for 5 min at 60 °C. After a thorough rinse with distilled water, the samples were etched in 10% HCl for 5 min to neutralize the remnants of alkaline solution and to activate the surface. Finally, the substrates were rinsed again with distilled water and dried by hot air. After surface preparations, to prevent formation of oxide layer on their surfaces, the samples were immediately placed in the plating bath. The electrolyte used for direct current (DC) electrodeposition contained 0.4 M ZnSO₄, 0.005–0.02 M CoSO₄, and 2 M glycine (NH₂CH₂COOH). The pH of electrolyte was adjusted to 11 by adding sodium hydroxide, and deposition was carried out at room temperature. The thickness of the coatings was fixed at approximately 12 μm.

Cyclic voltammetry and potentiodynamic polarization tests were carried out in a three-electrode cell using an EG&G potentiostat/galvanostat, model 273A. Platinum plate and saturated calomel electrode (SCE) were used as counter and reference electrodes, respectively. An AISI 1018 steel specimen that had been placed in a Teflon mounting material was also used as a working electrode. The potential scan in cyclic voltammetry study was started in the negative direction from -400 mV and reversed at -1400 mV in positive direction, at three different potential scan rates of 5, 10, and 15 mV s⁻¹. The potentiodynamic polarization tests were carried out in 3.5 wt% NaCl solution by sweeping the potential at a scan rate of 2 mV s⁻¹ from -1800 to 200 mV (vs. SCE). The working electrode

was kept in the 3.5 wt% NaCl solution for 30 min prior to establish the potential.

The surface morphologies of the coatings were characterized by SEM model MV-2300 and the chemical compositions of the coatings were determined via energy dispersive spectroscopy (EDS). The phase compositions of the coatings were also determined via XRD analysis using a diffractometer (model Philips X'Pert Pro) with Co K α radiation ($\lambda = 1.7889 \text{ \AA}$) at 30 kV and 20 mA. The 2θ ranged from 20° to 120° and the scan rate was 0.02° per second.

3 Results and discussions

3.1 Voltammetric studies

Figure 1 shows cyclic voltammograms of the specimens exposed to solutions containing Zn²⁺ or Co²⁺ alone and Zn²⁺ + Co²⁺ in the presence of glycine, at room temperature. The potential scan was started in the negative direction from -400 mV and reversed at -1400 mV in positive direction, while potential scan rate was 10 mV s⁻¹.

According to cyclic voltammogram of Co²⁺ alone (curve a in Fig. 1), the equilibrium potential of cobalt reduction moves toward more negative values at about -870 mV versus SCE and the growth of the deposited layer increases gradually when the potential shifts to more negative values. The transition of reduction potential to more negative values could be due to the formation of Co-glycine complex species [28, 29]. During potential scan in positive direction in cyclic voltammogram of cobalt, the anodic peak at the potential of about -570 mV versus

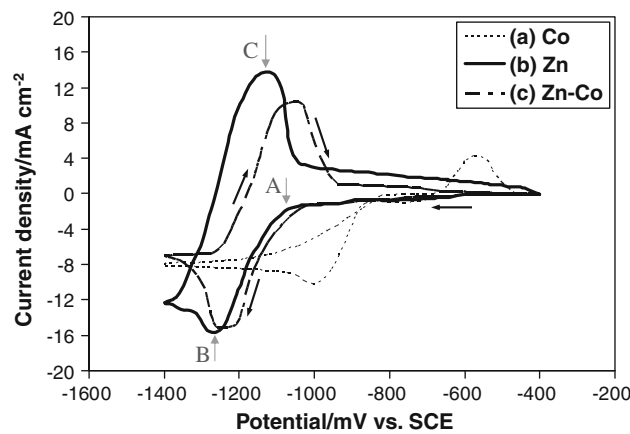


Fig. 1 Cyclic voltammograms for the electrodeposition on steel in 2 M glycine solutions with pH = 11 containing: a 0.005 M CoSO₄, b 0.4 M ZnSO₄, c 0.005 M CoSO₄, and 0.4 M ZnSO₄, at room temperature and scan rate of 10 mV s⁻¹

SCE, corresponds to the anodic dissolution of deposited cobalt.

According to cyclic voltammogram of Zn^{2+} alone (curve b in Fig. 1), after the first deposited spike that is located at the potential of about -1080 mV versus SCE (Point A), the current density increases. As a result, the deposited spikes will gradually develop and the following observed peak at potential of about -1260 mV versus SCE belongs to the bulk deposition of zinc (Point B). The revealed anodic peak at potential of about -1130 mV versus SCE (Point C) belongs to the dissolution of deposited zinc.

Observing the cyclic voltammogram of Zn–Co alloy (curve c in Fig. 1), it is found that the reduction process has happened in a certain peak at -1240 mV versus SCE that is attributed to simultaneous reduction of Zn^{2+} and Co^{2+} ions. This shows that glycine has acted as a suitable and successful complexing agent in co-deposition of Zn and Co. It is also found that deposition potential of Zn–Co alloy is closer to that of zinc rather than cobalt. This behavior is related to the presence of Zn^{2+} , which inhibits Co^{2+} reduction. Many researches [8, 29–32] have attributed this behavior to the underpotential deposition (UPD) of zinc on cobalt. A peak at potential -1070 mV versus SCE is located on the anodic part of the Zn–Co cyclic voltammogram that shows oxidation and dissolution of the deposited alloy. The potential of this peak is more positive than the dissolution potential of pure zinc and also the height of this peak (current peak) is smaller than the height of dissolution peak of pure zinc. It is therefore concluded that the main constituent of electrodeposited Zn–Co alloy is zinc with a small fraction of cobalt [2, 8].

Figure 2 shows cyclic voltammograms of the specimen exposed to electrolyte containing 2 M glycine + 0.4 M

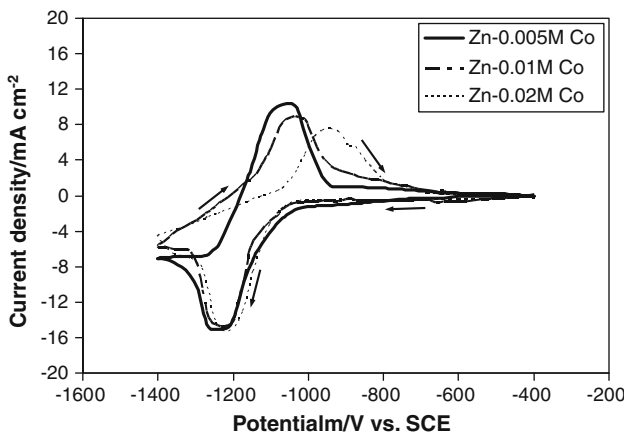


Fig. 2 Cyclic voltammograms for the electrodeposition from solutions containing: 0.4 M $ZnSO_4$ + 2 M glycine and three different $CoSO_4$ contents, with $pH = 11$ at room temperature and scan rate of 10 mV s^{-1}

$ZnSO_4$ and different concentrations of cobalt from 0.005 to 0.02 M with potential scan rate of 10 mV s^{-1} at room temperature. It is observed that the reduction potential of Zn–Co alloy does not change considerably, when cobalt concentration in electrolyte increases. It is also seen that in the anodic part of cyclic voltammetry, when cobalt concentration increases from 0.005 to 0.02 M , the anodic peak potential gradually moves toward more positive values and simultaneously, the anodic peak current reduces. These changes show that when cobalt concentration in electrolyte increases the amount of zinc in the alloy decreases and the formation of cobalt in the deposited alloy increases. Besides, by increasing of cobalt concentration in the electrolyte from 0.005 to 0.01 M , one anodic peak is only observed, that is an indication of solid solution of cobalt in zinc. In the electrolyte containing 0.02 M cobalt, a small anodic peak at potential of about -880 mV versus SCE is also observed that can be an indication of the formation of an intermetallic phase [8, 29, 33].

Figure 3 shows cyclic voltammograms obtained from the electrolyte containing 0.005 M $CoSO_4$, 0.4 M $ZnSO_4$, and 2 M glycine at three different scan rates of 5 , 10 , and 15 mV s^{-1} . It is observed that when scan rate increases from 5 to 15 mV s^{-1} , cathodic peak potential moves toward more negative values, and anodic peak potential moves toward more positive values. Therefore, with the increase of scan rate, the distance between anodic and cathodic peaks increases. This increase is related to the loss of ohmic drop [34]. Figure 3 also indicates that the reactions of reduction–oxidation (redox) in Zn–Co alloy are quasi-reversible, because the ratio of cathodic to anodic peak current is almost close to one [35].

Figure 4a and b shows the relation between cathodic and anodic peak current densities versus square root of scan

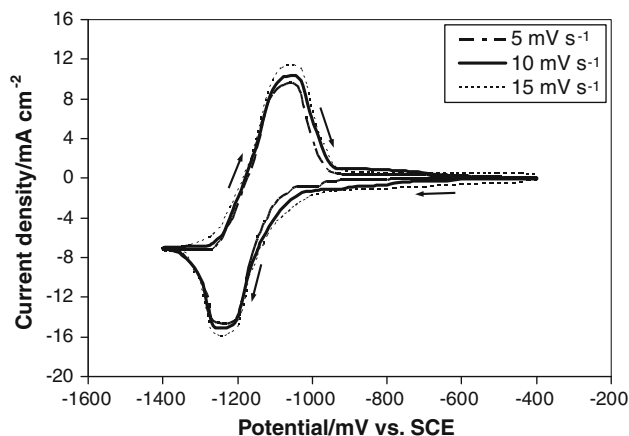


Fig. 3 Cyclic voltammograms for the electrodeposition on steel in electrolyte containing: 0.005 M $CoSO_4$, 0.4 M $ZnSO_4$, and 2 M glycine with $pH = 11$, at room temperature with different scan rates: 5 , 10 , and 15 mV s^{-1}

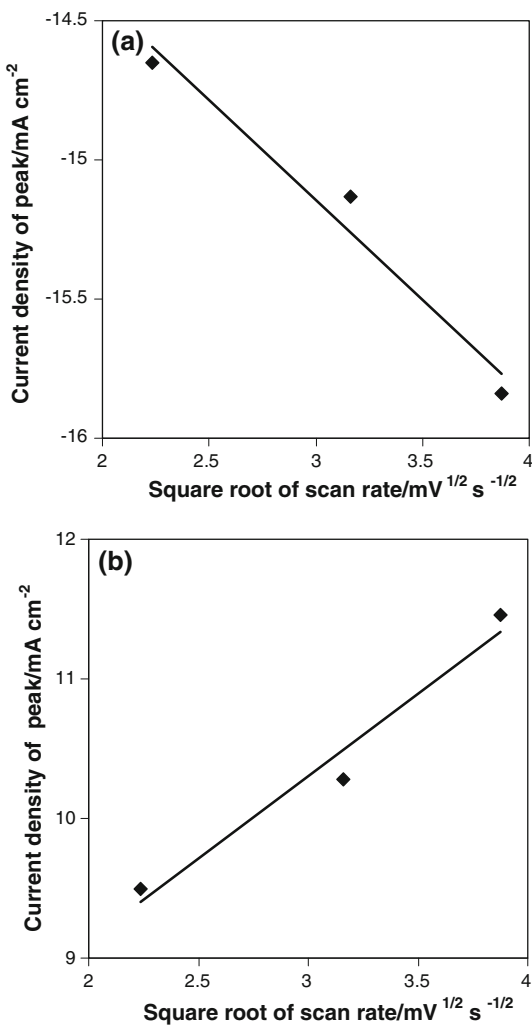


Fig. 4 Variations in current density of cathodic (a) and anodic (b) peaks with square root of scan rate in electrolyte containing: 0.005 M CoSO_4 , 0.4 M ZnSO_4 , and 2 M glycine with $\text{pH} = 11$, at room temperature

rate. There is a relatively good liner relationship between these currents and the square root of the scan rates. According to Randles–Sevcik equation, the cathodic and anodic peak currents in diffusion-controlled reversible or quasi-reversible electrochemical reactions are directly related to the square root of the potential scan rate [35–37]. Therefore, it appears that electrodeposition of Zn–Co alloy in alkaline bath containing glycine is controlled by diffusion mechanism.

3.2 Chemical composition and morphology of the deposits

Effect of current density on the cobalt content of the electrodeposits was investigated using a bath containing 0.4 M ZnSO_4 , 0.02 M CoSO_4 , and 2 M glycine. According to Fig. 5, by increasing current density, the Co content of

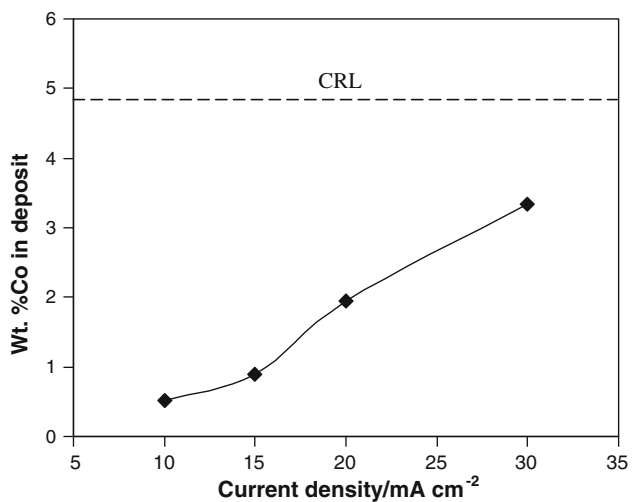


Fig. 5 Effect of current density on the Co content of Zn–Co alloy electrodeposits in electrolyte containing: 0.02 M CoSO_4 , 0.4 M ZnSO_4 , and 2 M glycine with $\text{pH} = 11$, at room temperature

the coating increases and approaches the composition reference line (CRL) which is defined according to Eq. 1 [17, 38, 39]:

$$\text{CRL} = \frac{c(\text{Co}^{2+})}{[c(\text{Co}^{2+} + \text{Zn}^{2+})]}, \quad (1)$$

where $c(\text{Co}^{2+})$ and $c(\text{Zn}^{2+})$ are the concentrations of Co and Zn ions in the electrolyte, respectively.

The lower Co content of the alloy coatings in comparison with the CRL is the result of the preferential deposition of the less noble metal (Zn) as compared with the more noble metal (Co) that results in anomalous deposition of Zn–Co alloy coatings. By increasing current density, deposition of zinc which is reduced more easily is accelerated. As a result, the solution that is next to the cathode is depleted from Zn^{2+} and causes more Co^{2+} to have opportunity for reduction, and hence, the cobalt content of coating increases (Fig. 5).

Figure 6a–d shows the surface morphologies of Zn–Co alloy deposits obtained from plating bath containing 0.4 M ZnSO_4 , 0.02 M CoSO_4 , and 2 M glycine at current densities of 10, 15, 20, and 30 mA cm^{-2} , respectively. According to Fig. 6a and b, with the increase in current density from 10 to 15 mA cm^{-2} , the grain size reduces. However, further increase in the current density from 15 to 30 mA cm^{-2} has a reverse effect and causes grain coarsening (Fig. 6c–d). It is postulated that with increase in current density, due to the rise in the overpotential, free energy for formation of new nuclei in Zn–Co alloy deposits increases that leads to higher nucleation rate, and hence formation of coatings with smaller grain size [21]. However, further increase in current density from 15 mA cm^{-2} to higher values, will result in creation of discrete large

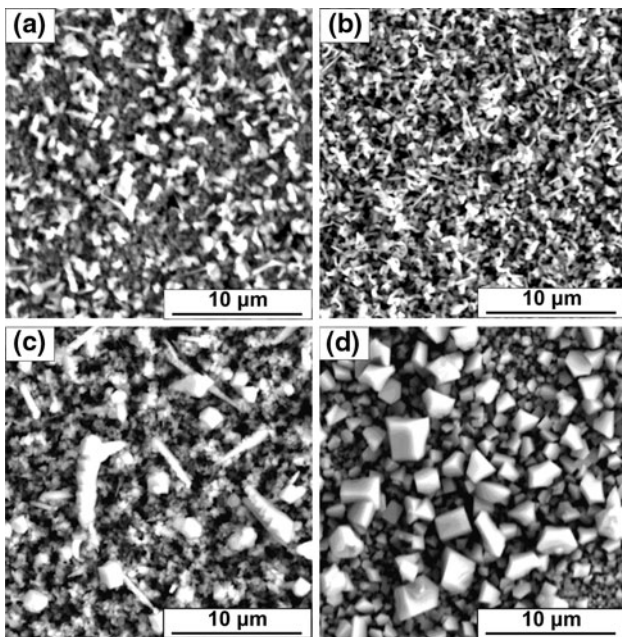


Fig. 6 Surface morphology of Zn–Co alloy coatings from electrolyte containing 0.02 M CoSO_4 , 0.4 M ZnSO_4 , and 2 M glycine at different current densities: **a** 10 mA cm^{-2} , **b** 15 mA cm^{-2} , **c** 20 mA cm^{-2} , and **d** 30 mA cm^{-2}

crystallites. The formation of large and discrete polyhedral grains is attributed to the fast growth of grains and agglomeration on the nuclei in comparing with nucleation rate [21, 29].

3.3 Phase composition of the deposits

X-Ray diffraction (XRD) patterns of pure zinc and Zn–Co alloy deposits obtained from electroplating bath containing 0.4 M ZnSO_4 , 0.02 M CoSO_4 , and 2 M glycine at different current densities are shown in Fig. 7. The presence of cobalt in the alloy coatings slightly decreases the intensities of the diffracted planes as compared with those of the pure zinc. With an increase in cobalt content in Zn–Co alloy deposits (due to an increase of current density), the intensity of peaks for planes (002), (100), and (101) decreases further. This decrease of intensity is also observed in other peaks related to hexagonal phase of zinc, but in a lower extent. The persistence of those peaks, although with lower intensity suggests the appearance of a zinc-rich phase (η) which is a solid solution of Co in Zn in these coatings. This decrease of intensity in peaks is the result of variation in orientation of the zinc crystallographic planes by virtue of increase in Co content of coating that causes the distortion of hexagonal structure of zinc [24, 29, 40]. By increasing the current density to more than 20 mA cm^{-2} during electroplating, and hence increase in the cobalt content in the deposits, a new phase called γ -phase (CoZn_{13}) is

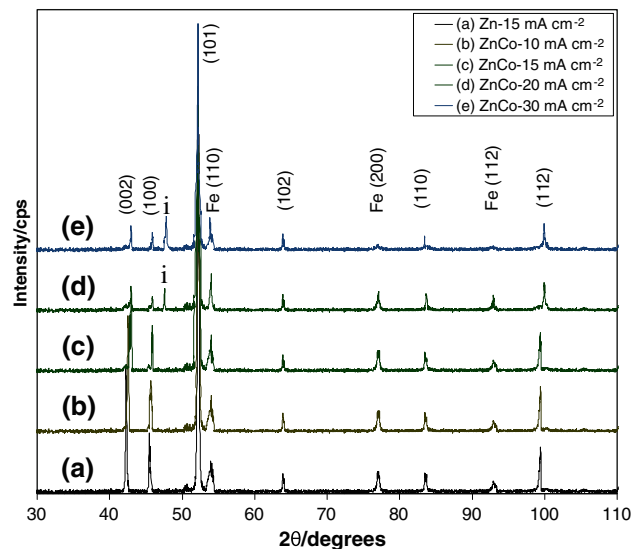


Fig. 7 XRD patterns obtained from (a) pure zinc coating from electrolyte containing: 0.4 M ZnSO_4 and 2 M glycine at 15 mA cm^{-2} and Zn–Co alloy coatings from electrolyte containing: 0.02 M CoSO_4 , 0.4 M ZnSO_4 , and 2 M glycine at different current densities: (b) 10 mA cm^{-2} , (c) 15 mA cm^{-2} , (d) 20 mA cm^{-2} and (e) 30 mA cm^{-2}

formed. The XRD patterns indicated as d and e in Fig. 7 shows the presence of this new phase indicated with letter i.

Overall, it appears that the structures of the electrodeposited Zn–Co alloy coatings deviate from the equilibrium phase diagrams. This behavior is attributed to quasi-reversible reactions in electrodeposition of Zn–Co alloys that were noticed in cyclic voltammetry studies.

Table 1 summarizes the effect of current density on chemical composition and phase composition of the alloy coatings (obtained from electroplating bath containing 0.4 M ZnSO_4 , 0.02 M CoSO_4 , and 2 M glycine) on which potentiodynamic polarization test were carried out.

3.4 Corrosion behaviors of the deposits

Figure 8 illustrates the polarization curves obtained from potentiodynamic polarization tests in 3.5 wt% NaCl solution for Zn–Co alloy coatings. Two stages of passivation are observed in Zn–Co alloy coatings. This can be an

Table 1 Effect of current density on chemical composition and phase composition of Zn–Co alloy coatings from electrolyte containing: 0.4 M ZnSO_4 , 0.02 M CoSO_4 , and 2 M glycine

Coating	Current density (mA cm^{-2})	Wt% Co in deposit	Phase composition
Zn–Co	10	0.52	η
Zn–Co	15	0.89	η
Zn–Co	20	1.95	$\gamma + \eta$
Zn–Co	30	3.34	$\gamma + \eta$

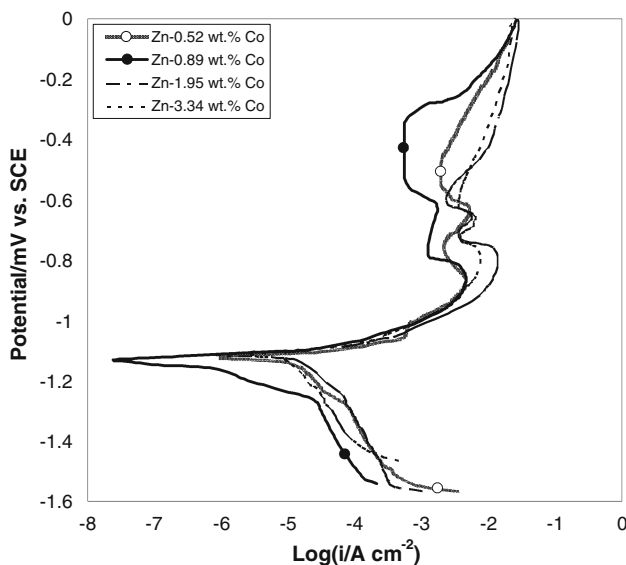
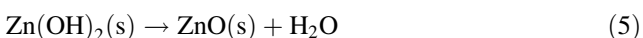
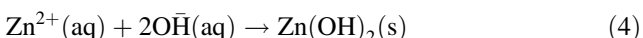


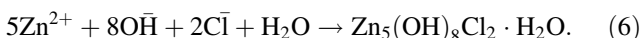
Fig. 8 Polarization curves obtained for Zn–Co alloy coatings from electrolyte containing: 0.02 M CoSO_4 , 0.4 M ZnSO_4 , and 2 M glycine with pH = 11, in 3.5% NaCl

indication of the formation of protective film in two stages. When Zn–Co alloy is corroded, zinc begins to dissolve preferentially according to Eqs. 2–5 [22, 41]:



Therefore, the protective films are complex compositions including $\text{Zn}(\text{OH})_2$ and ZnO that cover the surfaces of the corroded coatings and create areas in which current density is independent of potential.

The presence of cobalt in the coating enhances dissolution of zinc in NaCl solution. Consequently, the increase in zinc dissolution causes its reaction with chloride ions in NaCl solution and formation of zinc hydroxy chloride (ZHC) according to Eq. 6 [22, 42]:



ZHC has a very low product of solubility, and ensures higher protective ability for Zn–Co alloy coatings [42, 43].

The results obtained from polarization tests for Zn–Co alloy coatings are summarized in Table 2. The corrosion potential (E_{corr}) and corrosion current density (i_{corr}) calculated from the intersection of the cathodic and anodic Tafel slopes in the range of ± 50 mV of the open-circuit potential (E_{ooc}). It is noticed that Zn–0.89 wt% Co alloy coating has the lowest corrosion current density among coatings and creates the protective passive film with a wider passive range. Moreover, it is observed that passive current density of Zn–0.89 wt% Co alloy coating is lower than those of other coatings, indicating that this coating passivates much easier than other coatings. Therefore, Zn–0.89 wt% Co has the highest corrosion resistance among all coatings. It is also noticed that the protective passive film that is formed on the surface of Zn–0.52 wt% Co possesses widespread passive range that shows corrosion resistance of this coating is higher than those of Zn–Co alloy coatings with 1.95 and 3.34 wt% Co.

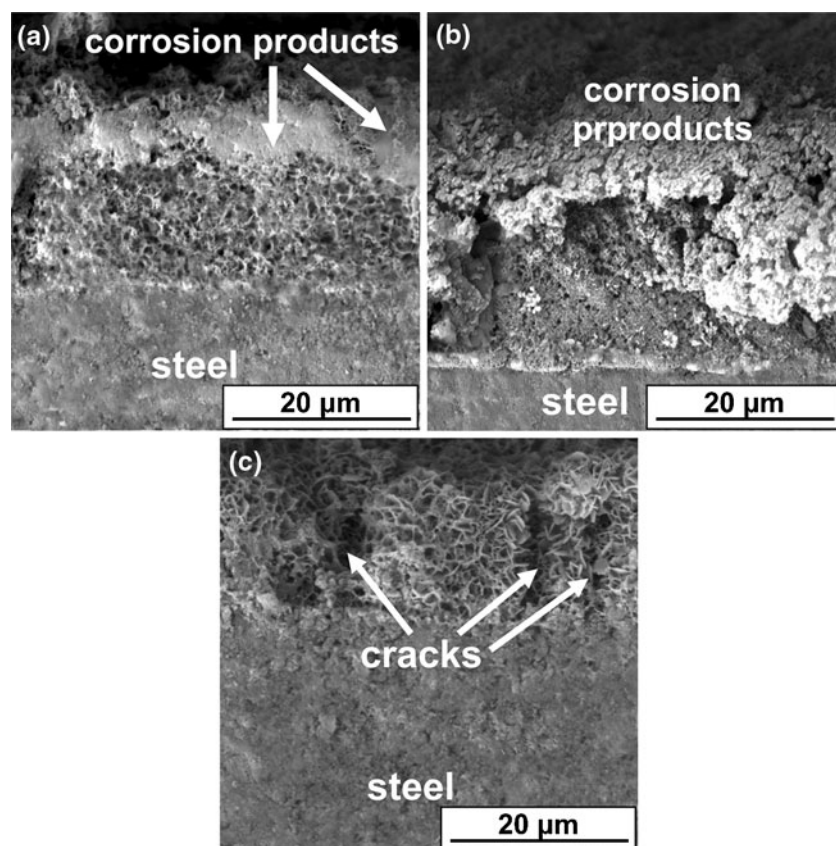
Zn–3.34 wt% Co alloy coating, possessed the lowest corrosion resistance compared to other alloy coatings and showed that the lowest passive range and the highest corrosion current density among the coatings. The lower corrosion resistance of Zn–Co alloy coatings with 1.95 and 3.34 wt% Co are due to their dual phase nature ($\eta + \gamma$) as confirmed by their XRD patterns (Fig. 6), that promotes galvanic corrosion. In alloy coatings with single phase structure (η -phase), i.e., the coatings with 0.52 and 0.89 wt% Co, the coating with smaller grain size (i.e., the one with 0.89 wt% Co) exhibited higher corrosion resistance than the coating with coarser grain size. This is due to the higher grain boundary density in the coating with smaller grain size that speeds up the formation of a stable and protective passive film. Similar behaviors have been reported by Youssef et al. [41] and Wang et al. [44] who worked on pure zinc and pure cobalt.

The cross-sectioned SEM images of Zn–Co alloy deposits after potentiodynamic polarization test followed by 10 h immersion in 3.5 wt% NaCl solution are shown in Fig. 9a–c. It is observed that surface of Zn–0.89 wt% Co alloy (Fig. 9b) is covered with corrosion products (mainly ZHC) that act as barriers against further corrosion. It is also noticed that in Zn–Co alloy coatings with 0.52 and 1.95 wt% Co, the corrosion damages in cross-section are in

Table 2 Variation of corrosion current density (i_{corr}), corrosion potential (E_{corr}), passive current density (i_{pass}), passivation potential (E_p), breakdown potential (E_b), and passive range ($E_b - E_p$) for various coatings, measured in 3.5 wt% NaCl solutions

Coating	i_{corr} ($\mu\text{A cm}^{-2}$)	E_{corr} (mV)	i_{pass} ($\mu\text{A cm}^{-2}$)	E_p (mV)	E_b (mV)	$E_b - E_p$ (mV)
Zn–0.52 wt% Co	12.59	−1124	2168	−774	−464	310
Zn–0.89 wt% Co	0.84	−1148	1298	−789	−326	463
Zn–1.95 wt% Co	15.85	−1135	3800	−721	−593	128
Zn–3.34 wt% Co	17.84	−1150	3880	−730	−609	121

Fig. 9 Cross-section micrographs of Zn–Co alloy coatings with: **a**: 0.52, **b**: 0.89, **c**: 1.95 wt% Co, after potentiodynamic polarization test followed by 10 h immersion in 3.5 wt% NaCl solution



the form of uneven pits and surface of these coatings is covered with discrete corrosion products. The pitting corrosion could be related to the absorption of halide anions on the passive films formed on the coatings. The anions that are absorbed on the passive film create an electrostatic field across the interface of passive film and electrolyte. When the electrostatic field reaches a critical value, the absorbed anions start to penetrate in the passive film especially at the point defects of the film. This process leads to breakdown of the passive film and causes local dissolution on surface of the passive film [45, 46]. Cross-sectioned micrograph of the Zn–1.95 wt% Co alloy coating shows cracks from the surface down to the substrate. The presence of such cracks is associated with the dissolution of zinc-rich phases.

4 Conclusions

1. The cyclic voltammetry reveals that glycine play a beneficial effect in electrodeposition of Zn–Co alloys, since the reduction potential of the Co^{2+} is brought close to that of the Zn^{2+} , so that co-deposition of cobalt and zinc successfully occurs.
2. The mechanism of Zn–Co alloy deposition in alkaline bath containing glycine is controlled by diffusion

mechanism. It is also shown that reduction–oxidation reactions in Zn–Co alloy deposits are quasi-reversible that results in deviation of electrodeposited alloys from the equilibrium phase diagrams.

3. Under the examined conditions, electrodeposition of the Zn–Co alloys is anomalous and increase in current density results in increase of cobalt in Zn–Co alloy electrodeposits.
4. Zn–Co alloy coatings with 1.95 and 3.34 wt% Co are consisted of two phases (η and γ), but Zn–Co alloy coatings with lower cobalt content have single phase structure (η -phase) which is a solid solution of cobalt in zinc.
5. Among alloy coatings with single phase structure (η -phase), the coating with smaller grain size (i.e., the one with 0.89 wt% Co) exhibited higher corrosion resistance than the coating with coarser grain size (i.e., the one with lower cobalt value of 0.52 wt%). This is due to the higher grain boundary density in the coating with smaller grain size that speeds up the formation of a stable and protective passive film. The lower corrosion resistance of Zn–Co alloy coatings with 1.95 and 3.34 wt% Co are due to their dual phase nature ($\eta + \gamma$), that promotes galvanic corrosion.

References

1. Sohi MH, Jalali M (2003) *J Mater Process Technol* 138:63
2. Roventi G, Bellezze T, Fratesi R (2006) *Electrochim Acta* 51:2691
3. Bajat JB, Miskovic-Stankovic VB, Kacarevic-Popovic Z (2002) *Prog Org Coat* 45:379
4. Boshkov N, Tsvetkova N, Petrov P, Koleva D, Petrov K, Avdeev G, Tsvetanov C, Raichevsky G, Raicheff R (2008) *Appl Surf Sci* 254:5618
5. Tomachuk CR, Freire CMA, Ballester M, Fratesi R, Roventi G (1999) *Surf Coat Technol* 122:6
6. Abou-Krisha MM, Rageh HM, Matter EA (2008) *Surf Coat Technol* 202:3739
7. Hillier EMK, Robinson MJ (2006) *Corros Sci* 48:1019
8. Abou-krisha MM, Abushoffa AM (2007) *Int J Electrochem Sci* 2:418
9. Zhang Z, Leng WH, Shao HB, Zhang JQ, Wang JM, Cao CN (2001) *J Electroanal Chem* 516:127
10. Diaz SL, Mattos OR, Barcia OE, Fabri Miranda FJ (2002) *Electrochim Acta* 47:4091
11. Yang ZN, Zhang Z, Zhang JQ (2006) *Surf Coat Technol* 200:4810
12. Gomez E, Pelaez E, Valles E (1999) *J Electroanal Chem* 469:139
13. Gomez E, Alcobe X, Valles E (1999) *J Electroanal Chem* 475:66
14. Ashassi-Sorkhabi H, Haghighi A, Parvini-Ahmadi N, Manzoori J (2001) *Surf Coat Technol* 140:278
15. Abou-Krisha MM (2005) *Appl Surf Sci* 252:1035
16. Hillier EMK, Robinson MJ (2004) *Corros Sci* 46:715
17. Lodhi ZF, Mol JMC, Hamer WJ, Terryn HA, De Wit JHW (2007) *Electrochim Acta* 52:5444
18. Ramanauskas R, Muleshkova L, Maldonado L, Dobrovolskis P (1998) *Corros Sci* 40:401
19. Lan CJ, Liu WY, Ke ST, Chin TS (2006) *Surf Coat Technol* 201:3103
20. Hosseini MG, Ashassi-Sorkhabi H, Ghiasvand HAY (2008) *Surf Coat Technol* 202:2897
21. Ramanauskas R, Gudaviciute L, Juskenas R (2008) *Chemija* 19:7
22. Neto PDL, Correia AN, Colares RP, Araujo WS (2007) *J Braz Chem Soc* 18:1164
23. Mouanga M, Ricq L, Ismaili L, Refouelet B, Bercot P (2007) *Surf Coat Technol* 201:7143
24. Mouanga M, Ricq L, Bercot P (2008) *Surf Coat Technol* 202:1645
25. Mouanga M, Ricq L, Douglade G, Douglade J, Bercot P (2006) *Surf Coat Technol* 201:762
26. Barbosa LL, Carlos IA (2006) *Surf Coat Technol* 201:1695
27. Ballesteros JC, Diaz-Arista P, Meas Y, Ortega R, Trejo G (2007) *Electrochim Acta* 52:3686
28. Rashwan SM (2005) *Mater Chem Phys* 89:192
29. Ortiz-Aparicio JL, Meas Y, Trejo G, Ortega R, Chapman TW, Chainet E, Ozil P (2007) *Electrochim Acta* 52:4742
30. Nicol MJ, Philip HI (1976) *J Electroanal Chem* 70:233
31. Swathirajan S (1987) *J Electroanal Chem* 221:211
32. Chen PY, Sun IW (2001) *Electrochim Acta* 46:1169
33. Gomez E, Alcobe X, Valles E (2001) *J Electroanal Chem* 505:54
34. Van Den Bos C, Schnitger HC, Zhang X, Hovestad A, Terryn H, De Wit JHW (2006) *Corros Sci* 48:1483
35. Feng G, Xiong Y, Wang H, Yang Y (2008) *Electrochim Acta* 53:8253
36. Mahajan RK, Vohra KK, Shaheen A, Aswal VK (2008) *J Colloid Interface Sci* 326:89
37. Grujicic D, Pesic B (2005) *Electrochim Acta* 50:4426
38. Lodhi ZF, Mol JMC, Hovestad A, Terryn H, De Wit JHW (2007) *Surf Coat Technol* 202:84
39. Lichusina S, Chodosovskaja A, Sudavicius A, Juskenas R, Bucinskienė D, Seiskis A, Juzeliunas E (2008) *Chemija* 19:25
40. Ramanauskas R (1999) *Appl Surf Sci* 153:53
41. Youssef KMS, Koch CC, Fedkiw PS (2004) *Corros Sci* 46:51
42. Boshkov N, Petrov K, Vitkova S, Nemška S, Raichevsky G (2002) *Surf Coat Technol* 157:171
43. Boshkov N, Petrov K, Kovacheva D, Vitkova S, Nemška S (2005) *Electrochim Acta* 51:77
44. Wang L, Lin Y, Zeng Z, Liu W, Xue Q, Hu L, Zhang J (2007) *Electrochim Acta* 52:4342
45. Assaf FH, Abd El-Rehieem SS, Zaky AM (1999) *Mater Chem Phys* 58:58
46. Li MC, Royer M, Stien D, Lecante A, Roos C (2008) *Corros Sci* 50:1975